This manuscript was accepted by Appl. Phys. Lett. Click here to see the version of record.

Low spin wave damping in the insulating chiral magnet Cu_2OSeO_3

I. Stasinopoulos,[1] S. Weichselbaumer,[1] A. Bauer,[2] J. Waizner,[3]
H. Berger,[4] S. Maendl,[1] M. Garst,[3,5] C. Pfleiderer,[2] and D. Grundler[6,*]

[1] *Physik Department E10, Technische Universität München, D-85748 Garching, Germany*
[2] *Physik Department E51, Technische Universität München, D-85748 Garching, Germany*
[3] *Institute for Theoretical Physics, Universität zu Köln, D-50937 Köln, Germany*
[4] *Institut de Physique de la Matière Complexe, École Polytechnique Fédérale de Lausanne, 1015 Lausanne, Switzerland*
[5] *Institut für Theoretische Physik, Technische Universität Dresden, D-01062 Dresden, Germany*
[6] *Institute of Materials (IMX) and Laboratory of Nanoscale Magnetic Materials and Magnonics (LMGN), École Polytechnique Fédérale de Lausanne (EPFL), Station 12, 1015 Lausanne, Switzerland*

(Dated: July 7, 2017)

Chiral magnets with topologically nontrivial spin order such as Skyrmions have generated enormous interest in both fundamental and applied sciences. We report broadband microwave spectroscopy performed on the insulating chiral ferrimagnet Cu_2OSeO_3. For the damping of magnetization dynamics we find a remarkably small Gilbert damping parameter of about 1×10^{-4} at 5 K. This value is only a factor of 4 larger than the one reported for the best insulating ferrimagnet yttrium iron garnet at room temperature. We detect a series of sharp resonances and attribute them to confined spin waves in the mm-sized samples. Considering the small damping, insulating chiral magnets turn out to be promising candidates when exploring non-collinear spin structures for high frequency applications.

PACS numbers: 76.50.+g, 74.25.Ha, 4.40.Az, 41.20.Jb

The development of future devices for microwave applications, spintronics and magnonics [1–3] requires materials with a low spin wave (magnon) damping. Insulating compounds are advantageous over metals for high-frequency applications as they avoid damping via spin wave scattering at free charge carriers and eddy currents [4, 5]. Indeed, the ferrimagnetic insulator yttrium iron garnet (YIG) holds the benchmark with a Gilbert damping parameter $\alpha_{\rm intr} = 3 \times 10^{-5}$ at room temperature [6, 7]. During the last years chiral magnets have attracted a lot of attention in fundamental research and stimulated new concepts for information technology [8, 9]. This material class hosts non-collinear spin structures such as spin helices and Skyrmions below the critical temperature T_c and critical field H_{c2} [10–12]. Dzyaloshinskii-Moriya interaction (DMI) is present that induces both the Skyrmion lattice phase and nonreciprocal microwave characteristics [13]. Low damping magnets offering DMI would generate new prospects by particularly combining complex spin order with long-distance magnon transport in high-frequency applications and magnonics [14, 15]. At low temperatures, they would further enrich the physics in magnon-photon cavities that call for materials with small $\alpha_{\rm intr}$ to achieve high-cooperative magnon-to-photon coupling in the quantum limit [16–19].

In this work, we investigate the Gilbert damping in Cu_2OSeO_3, a prototypical insulator hosting Skyrmions [20–23]. This material is a local-moment ferrimagnet with $T_c = 58$ K and magnetoelectric coupling [24] that gives rise to dichroism for microwaves [25–27]. The magnetization dynamics in Cu_2OSeO_3 has already been explored [13, 28, 29]. A detailed investigation on the damping which is a key quality for magnonics and spintronics has not yet been presented however. To evaluate $\alpha_{\rm intr}$ we explore the field polarized state (FP) where the two spin sublattices attain the ferrimagnetic arrangement [21]. Using spectra obtained by two different coplanar waveguides (CPWs), we extract a minimum $\alpha_{\rm intr}=(9.9 \pm 4.1)\times10^{-5}$ at 5 K, i.e. only about four times higher than in YIG. We resolve numerous sharp resonances in our spectra and attribute them to modes that are confined modes across the macroscopic sample and allowed for by the low damping. Our findings substantiate the relevance of insulating chiral magnets for future applications in magnonics and spintronics.

From single crystals of Cu_2OSeO_3 we prepared two bar-shaped samples exhibiting different crystallographic orientations. The samples had lateral dimensions of $2.3 \times 0.4 \times 0.3\,{\rm mm}^3$. They were positioned on CPWs that provided us with a radiofrequency (rf) magnetic field **h** induced by a sinusoidal current applied to the signal surrounded by two ground lines (Fig. 1 and Supplementary Tab. (SI)). We used two different CPWs with either a

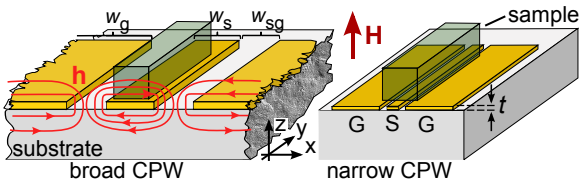

FIG. 1. Sketch of a single crystal mounted on either a broad or narrow CPW with a signal (S) line width w_s of either 1 mm or 20 μm, respectively (not to scale). The rf field **h** is indicated. The static field **H** is applied perpendicular to the CPW plane.

broad [30] or narrow signal line width of $w_s = 1\,\mathrm{mm}$ or $20\,\mu\mathrm{m}$, respectively. The central long axis of the rectangular Cu_2OSeO_3 rods was positioned on the central axis of the CPWs. The static magnetic field $\mathbf{H}$ was applied perpendicular to the substrate with $\mathbf{H} \parallel \langle 100\rangle$ and $\mathbf{H} \parallel \langle 111\rangle$ for sample S1 and S2, respectively. The direction of H defined the z-direction following the definition of Ref. [4]. The rf field component $\mathbf{h} \perp \mathbf{H}$ provided the relevant torque for excitation. Components $\mathbf{h} \parallel \mathbf{H}$ did not induce precessional motion in the FP state of Cu_2OSeO_3. We recorded spectra by a vector network analyzer using the magnitude of the scattering parameter S_{12}. We subtracted a background spectrum recorded at 1 T to enhance the signal-to-noise ratio (SNR) yielding the displayed $\Delta|S_{12}|$. In Ref. [7], Klingler *et al.* have investigated the damping of the insulating ferrimagnet YIG and found that Gilbert parameters α_{intr} evaluated from both the uniform precessional mode and standing spin waves confined in the macroscopic sample provided the same values. We evaluated damping parameters as follows (and further outlined in the Supplementary Material) [31]. When performing frequency-swept measurements at different fields H, the obtained linewidth Δf was considered to scale linearly with the resonance frequency f_r as [32]

$$\Delta f = 2\alpha_{\mathrm{intr}} \times f_r + \Delta f_0, \qquad (1)$$

with the inhomogeneous broadening Δf_0. In Fig. 2 (a) to (d) we show spectra recorded at 5 K in the FP state of the material using the two different CPWs. For the same applied field H we observe peaks residing at higher frequency f for $\mathbf{H} \parallel \langle 100\rangle$ compared to $\mathbf{H} \parallel \langle 111\rangle$. From the resonance frequencies, we extract the cubic magnetocrystalline anisotropy constant $K = (-0.6 \pm 0.1) \times 10^3\,\mathrm{J/m^3}$ for Cu_2OSeO_3 [compare Supplementary Fig. S1 and Supplementary Eqs. (S1) to (S3)]. The magnetic anisotropy energy is found to be extremal for $\langle 100\rangle$ and $\langle 111\rangle$ reflecting easy and hard axes. The saturation magnetization of Cu_2OSeO_3 amounted to $\mu_0 M_s = 0.13$ T at 5 K [22].

Figure 2 summarizes spectra taken with two different CPWs on the two different Cu_2OSeO_3 crystals S1 and S2 exhibiting different crystallographic orientation in the field H (further spectra are depicted in Supplementary Figs. S2). For the broad CPW [Fig. 2 (a) and (c)], we measured pronounced peaks whose linewidths were small. We resolved small resonances below the large peaks [arrows in Fig. 2 (b)] that shifted with H and exhibited an almost field-independent frequency offset δf from the main peaks that we will discuss later. For the narrow CPW [Fig. 2 (b) and (d)], we observed a broad peak superimposed by a series of resonances that all shifted to higher frequencies with increasing H. The field dependence excluded them from being noise or artifacts of the setup. Their number and relative intensities varied from sample to sample and also upon remounting the same sample in the cryostat (not shown). They disappeared with increasing temperature T but the broad peak remained. It is instructive to first follow the orthodox approach [29] and analyze damping parameters from modes reflecting the excitation characteristics of the broad CPW. Second, we follow Ref. [7] and analyze confined modes.

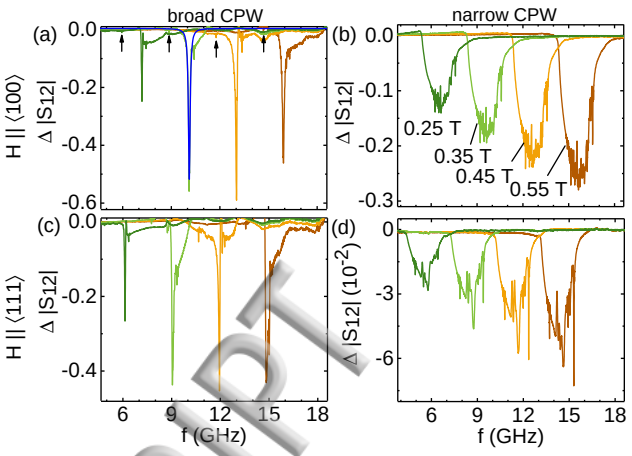

FIG. 2. (Color online) Spectra $\Delta|S_{12}|$ obtained at T = 5 K for different $\mathbf{H}$ using (a) a broad and (b) narrow CPW when $\mathbf{H}||\langle 100\rangle$ on sample S1. Corresponding spectra taken on sample S2 for $\mathbf{H}||\langle 111\rangle$ are shown in (c) and (d), respectively. Note the strong and sharp resonances in (a) and (c) when using the broad CPW that provides a much more homogeneous excitation field $\mathbf{h}$. Arrows mark resonances that have a field-independent offset with the corresponding main peaks and are attributed to standing spin waves. An exemplary Lorentz fit curve is shown in blue color in (a).

Lorentz curves (blue) were fitted to the spectra recorded with the broad CPW to determine resonance frequencies and linewidths. Note that the corresponding linewidths were larger by a factor of $\sqrt{3}$ compared to the linewidth Δf that is conventionally extracted from the imaginary part of the scattering parameters [33]. The extracted linewidths Δf were found to follow linear fits based on Eq. (1) at different temperatures [(Supplementary Figs. S2 and S3 (a)].

In Fig. 3 (a) we depict the parameter α_{intr} obtained from the broad CPW [34]. For $\mathbf{H} \parallel \langle 100\rangle$ [Fig. 3 (a)], between 5 and 20 K the lowest value for α_{intr} amounts to $(3.7 \pm 0.4) \times 10^{-3}$. This value is three times lower compared to preliminary data presented in Ref. [29]. Beyond 20 K the damping is found to increase. For $\mathbf{H} \parallel \langle 111\rangle$ we extract $(0.6 \pm 0.6) \times 10^{-3}$ as the smallest value. Note that these values for α_{intr} still contain an extrinsic contribution due to the inhomogeneity of $\mathbf{h}$ in z-direction and thus represent upper bounds for Cu_2OSeO_3. For the inhomogeneous broadening Δf_0 in Fig. 3 (b) the datasets taken with $\mathbf{H}$ applied along different crystal directions are consistent and show the smallest Δf_0 at lowest temperature. Note that a CPW wider than the

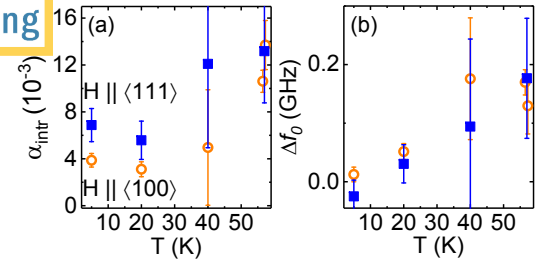

FIG. 3. (Color online) (a) Damping parameters $\alpha_{\rm intr}$ and (b) inhomogeneous broadening Δf_0 for **H** parallel to <100> (circle) and <111> (square). $\alpha_{\rm intr}$ and Δf_0 are obtained from the slopes and intercepts at $f_{\rm r} = 0$, respectively, of linear fits to the linewidth data (compare Supplementary Figs. S2 and S3.)

sample is assumed to excite homogeneously the ferromagnetic resonance (FMR) at $f_{\rm FMR}$ [35] transferring an in-plane wave vector $k = 0$ to the sample. Accordingly we ascribe the intense resonances of Fig. 2 (b) and (d) to $f_{\rm FMR}$. Using $f_{\rm FMR} = 6$ GHz and $\alpha_{\rm intr} = 3.7 \times 10^{-3}$ at 5 K [Fig. 3 (a)], we estimate a minimum relaxation time of $\tau = [2\pi\alpha_{\rm intr} f_{\rm r}]^{-1} = 6.6$ ns.

In the following, we examine in detail the additional sharp resonances that we observed in spectra of Fig. 2. In Fig. 2 (b) taken with the broad CPW for **H** $\parallel \langle 100\rangle$, we identify sharp resonances that exhibit a characteristic frequency offset δf with the main resonance at all fields (black arrows). We illustrate this in Fig. 4(a) in that we shift spectra of Fig. 2 (b) so that the positions of their main resonances overlap. The additional small resonances (arrows) in Fig. 2 (b) are well below the uniform mode. This is characteristic for backward volume magnetostatic spin waves (BVMSWs). Standing waves of such kind can develop if they are reflected at least once at the bottom and top surfaces of the sample. The resulting standing waves exhibit a wave vector $k = n\pi/d$, with order number n and sample thickness $d = 0.3$ mm. The BVMSW dispersion relation $f(k)$ of Ref. [13] (compare also Supplementary Fig. S4) provides a group velocity $v_{\rm g} = -300$ km/s at $k = \pi/d$ [triangles in Fig. 4 (b)]. The decay length $l_{\rm d} = v_{\rm g}\tau$ amounts to 2 mm considering $\tau = 6.6$ ns. This is about seven times larger than the relevant thickness d, thereby allowing standing spin wave modes to form across the thickness of the sample. Based on the dispersion relation of Ref. [13], we calculated the frequency splitting $\delta f = f_{\rm FMR} - f(n\pi/d)$ [open diamonds in Fig. 4 (inset)] assuming $n = 1$ and $t = 0.4$ mm for the sample width t defined in Ref. [13]. Experimental values (filled symbols) agree with the calculated ones (open symbols) within about 60 MHz. In case of the narrow CPW, that provides a broad wave vector distribution [36] we observe even more sharp resonances [Fig. 2 (a) and (c)]. A set of resonances was reported previously in the field-polarized phase of Cu_2OSeO_3 [26, 28, 37, 38]. Maisuradze *et al.* assigned secondary peaks in thin plates of Cu_2OSeO_3 to different standing spin-wave modes [38] in agreement with our analysis outlined above.

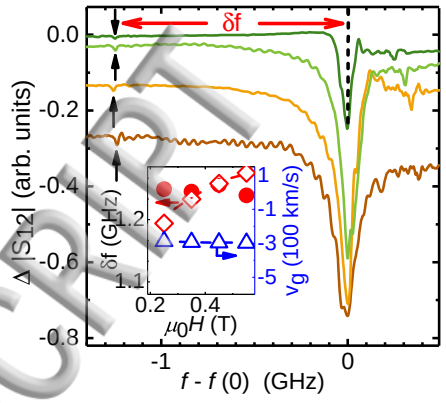

FIG. 4. (Color online) Spectra of Fig. 2 (b) replotted as $f - f_{\rm FMR}(H)$ for different H such that all main peaks are at zero frequency and the field-independent frequency splitting δf becomes visible. The numerous oscillations seen particularly on the bottom most curve are artefacts from the calibration routine. The inset depicts experimentally evaluated (filled circles) and theoretically predicted (diamonds) values δf using dispersion relations for a platelet. Calculated group velocity $v_{\rm g}$ at $k = \pi/(0.3$ mm). Dashed lines are guides to the eyes.

We attribute the series of sharp resonances in Fig. 2 (b) and (d) to further standing spin waves. In Fig. 5 (a) and (b) we highlight prominent and particularly narrow resonances with #1, #2 and #3 recorded with the narrow CPW for **H** $\parallel \langle 100\rangle$ and **H** $\parallel \langle 111\rangle$, respectively. We trace their frequencies $f_{\rm r}$ as a function of H. They depend linearly on H showing that for both crystal orientations the selected sharp peaks reflect distinct spin excitations. From the slopes we extract a Landé factor $g = 2.14$ at 5 K. Consistently, this value is slightly larger than $g = 2.07$ reported for 30 K in Ref. [13]. From $g = 2.14$ we calculate a gyromagnetic ratio $\gamma = g\mu_{\rm B}/\hbar = 1.88 \times 10^{11}$ rad/sT where $\mu_{\rm B}$ is the Bohr magneton of the electron. Note that the different metallic CPWs of Fig. 1 vary the boundary conditions and thereby details of the spin wave dispersion relations in Cu_2OSeO_3. However, the frequencies covered by dispersion relations vary only over a specific regime; for e.g. forward volume waves the regime even stays the same for different boundary conditions [4]. Following Klingler et al. [7] the exact mode nature and resonance frequency were not decisive when extracting Gilbert parameter.

We now concentrate on mode #1 in Fig. 5 (a) for **H** $\parallel$

⟨100⟩ at 5 K that is best resolved. We fit a Lorentzian lineshape as shown in Fig. 5(c) for 0.85 T, and summarize the corresponding linewidths Δf in Fig. 5(d). The inset of Fig. 5(d) shows the effective damping $\alpha_{\rm eff} = \Delta f/(2f_{\rm r})$ evaluated directly from the linewidth as suggested in Ref. [29]. We find that $\alpha_{\rm eff}$ approaches a value of about 3.5 $\times 10^{-4}$ with increasing frequency. This value is a factor of 10 smaller compared to $\alpha_{\rm intr}$ in Fig. 3 (a) extracted from FMR peaks by means of Eq. 1. This finding is interesting as $\alpha_{\rm eff}$ might still be enlarged by inhomogeneous broadening. To determine the intrinsic Gilbert-type damping from standing spin waves, we apply a linear fit to the linewidths Δf in Fig. 5(d) at $f_{\rm r} > 10.6$ GHz and obtain $(9.9 \pm 4.1)\times 10^{-5}$. For $f_{\rm r} \leq 10.6$ GHz the resonance amplitudes of mode #1 were small reducing the confidence of the fitting procedure. Furthermore, at low frequencies, we expect anisotropy to modify the extracted damping, similar to the results in Ref. [39]. For these reasons, the two points at low $f_{\rm r}$ were left out for the linear fit providing $\alpha'_{\rm intr} = (9.9 \pm 4.1)\times 10^{-5}$.

We find Δf and the damping parameters of Fig. 3 to increase with T. It does not scale linearly for $\mathbf{H} \parallel \langle 100\rangle$. A deviation from linear scaling was reported for YIG single crystals as well and accounted for by the confluence of a low-k magnon with a phonon or thermally excited magnon [5]. We now comment on our spectra taken with the broad CPW that do not show the very small linewidth attributed to the confined spin waves. The sharp mode #1 yields $\Delta f = 15.3$ MHz at $f_{\rm r} = 16.6$ GHz [Fig. 5 (d)]. At 5 K the dominant peak measured at 0.55 T and $f_{\rm r} = 15.9$ GHz with the broad CPW provides however $\Delta f = 129$ MHz. Δf obtained by the broad CPW is thus increased by a factor of eight. This increase is attributed to the finite distribution of wave vectors provided by the CPW. We confirmed this larger value on a third sample with $\mathbf{H} \parallel \langle 100\rangle$ and obtained $(3.1 \pm 0.3)\times 10^{-3}$ using the broad CPW (Supplementary Fig. S2). The discrepancy with the damping parameter extracted from the sharp modes of Fig. 5 might be due to the remaining inhomogeneity of $\mathbf{h}$ over the thickness of the sample leading to an uncertainty in the wave vector in z-direction. For a standing spin wave such an inhomogeneity does not play a role as the boundary conditions discretize k. Accordingly, Klingler *et al.* extracted the smallest damping parameter of $2.7(5) \times 10^{-5}$ reported so far for the ferrimagnet YIG at room temperature when analyzing confined magnetostatic modes [7]. The finding of Klingler *et al.* is consistent with the discussion in Ref. [33]. From Ref. [33] one can extract that the evaluation of damping from finite-wave-vector spin waves provides a damping parameter that is either equal or somewhat larger than the parameter extracted from the uniform mode (Supplementary material). The evaluation of Fig. 5 (d) thus overestimates the parameter.

To summarize, we investigated the spin dynamics in the field-polarized phase of the insulating chiral magnet Cu_2OSeO_3. We detected numerous sharp resonances

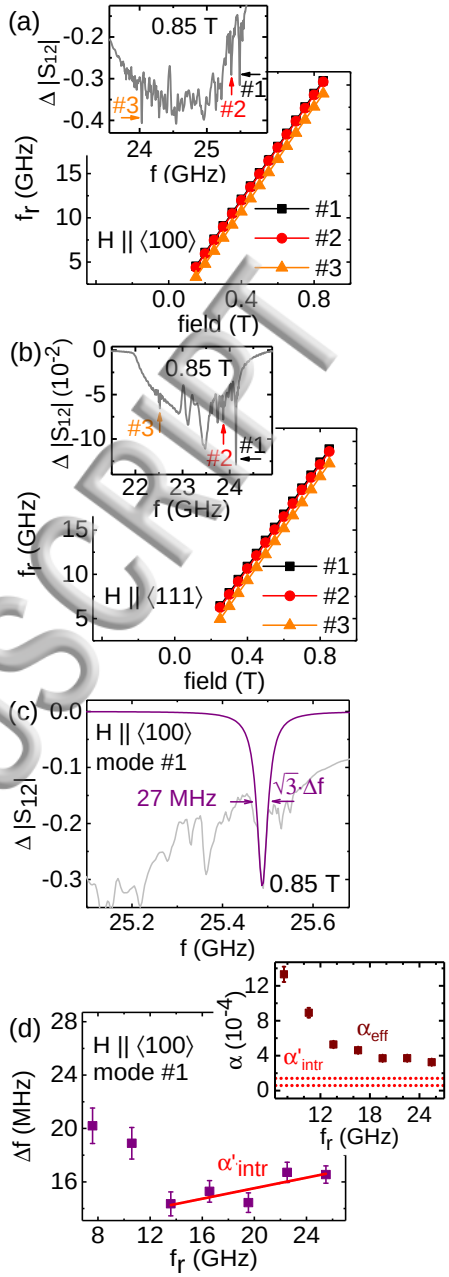

FIG. 5. (Color online) Resonance frequencies as a function of field H of selected sharp modes labelled #1 to #3 extracted from individual spectra (insets) for (a) $\mathbf{H} \parallel \langle 100\rangle$ and (b) $\mathbf{H} \parallel \langle 111\rangle$ at T = 5 K. (c) Lorentz fit of a sharp mode #1 for $\mathbf{H} \parallel \langle 100\rangle$ at 0.85 T. (d) Extracted linewidth Δf as a function of resonance frequency $f_{\rm r}$ along with the linear fit performed to determine the intrinsic damping $\alpha'_{\rm intr}$ from confined modes. Inset: Effective damping $\alpha'_{\rm eff}$ as a function of resonance frequency $f_{\rm r}$. The red dotted lines mark the error margins of $\alpha'_{\rm intr} = (9.9 \pm 4.1) \times 10^{-5}$.

that we attribute to standing spin waves. Their effective damping parameter is small and amounts to 3.5×10^{-4}. A quantitative estimate of the intrinsic Gilbert damping parameter extracted from the confined modes provides $(9.9 \pm 4.1) \times 10^{-5}$ at 5 K. The small damping makes an insulating ferrimagnet exhibiting Dzyaloshinskii-Moriya interaction a promising candidate for exploitation of complex spin structures and related nonreciprocity in magnonics and spintronics.

SUPPLEMENTARY MATERIAL

See supplementary material for further spectra, the magnetic anisotropy constant and linewidth evaluation.

ACKNOWLEDGMENT

We thank S. Mayr for assistance with sample preparation. Financial support through DFG TRR80 (projects E1 and F7), DFG FOR960, and ERC Advanced Grant 291079 (TOPFIT) is gratefully acknowledged.

* Electronic mail: dirk.grundler@epfl.ch

[1] I. Zutic and H. Dery, Nat. Mater. **10**, 647 (2011).
[2] M. Krawczyk and D. Grundler, J. Phys.: Condens. Matter **26**, 123202 (2014).
[3] A. V. Chumak, V. I. Vasyuchka, A. A. Serga, and B. Hillebrands, Nat. Phys. **11**, 453 (2015).
[4] A. G. Gurevich and G. A. Melkov, *Magnetization Oscillations and Waves* (CRC Press, 1996).
[5] M. Sparks, *Ferromagnetic-Relaxation Theory* (McGraw-Hill, 1964).
[6] A. A. Serga, A. V. Chumak, and B. Hillebrands, Journal of Physics D: Applied Physics **43**, 264002 (2010).
[7] S. Klingler, H. Maier-Flaig, C. Dubs, O. Surzhenko, R. Gross, H. Huebl, S. T. B. Goennenwein, and M. Weiler, Appl. Phys. Lett. **110**, 092409 (2017), http://dx.doi.org/10.1063/1.4977423.
[8] A. Fert, V. Cros, and J. Sampaio, Nat. Nanotechn. **8**, 152 (2013).
[9] N. Nagaosa and Y. Tokura, Nat. Nanotechn. **8**, 899 (2013).
[10] S. Mühlbauer, B. Binz, F. Jonietz, C. Pfleiderer, A. Rosch, A. Neubauer, R. Georgii, and P. Böni, Science **323**, 915 (2009).
[11] X. Z. Yu, Y. Onose, N. Kanazawa, J. H. Park, J. H. Han, Y. Matsui, N. Nagaosa, and Y. Tokura, Nature (London) **465**, 901 (2010).
[12] S. Seki, X. Z. Yu, S. Ishiwata, and Y. Tokura, Science **336**, 198 (2012).
[13] S. Seki, Y. Okamura, K. Kondou, K. Shibata, M. Kubota, R. Takagi, F. Kagawa, M. Kawasaki, G. Tatara, Y. Otani, and Y. Tokura, Phys. Rev. B **93**, 235131 (2016).
[14] M. Mochizuki and S. Seki, J. Phys.: Cond. Matter **27**, 503001 (2015).
[15] M. Garst, J. Waizner, and D. Grundler, J. Phys. D: Appl. Phys. (2017), http://iopscience.iop.org/10.1088/1361-6463/aa7573.
[16] H. Huebl, C. W. Zollitsch, J. Lotze, F. Hocke, M. Greifenstein, A. Marx, R. Gross, and S. T. B. Goennenwein, Phys. Rev. Lett. **111**, 127003 (2013).
[17] Y. Tabuchi, S. Ishino, T. Ishikawa, R. Yamazaki, K. Usami, and Y. Nakamura, Phys. Rev. Lett. **113**, 083603 (2014).
[18] X. Zhang, C.-L. Zou, L. Jiang, and H. X. Tang, Phys. Rev. Lett. **113**, 156401 (2014).
[19] M. Goryachev, W. G. Farr, D. L. Creedon, Y. Fan, M. Kostylev, and M. E. Tobar, Phys. Rev. Appl. **2**, 054002 (2014).
[20] K. Kohn, J. Phys. Soc. Jpn **42**, 2065 (1977).
[21] M. Belesi, I. Rousochatzakis, H. C. Wu, H. Berger, I. V. Shvets, F. Mila, and J. P. Ansermet, Phys. Rev. B **82**, 094422 (2010).
[22] T. Adams, A. Chacon, M. Wagner, A. Bauer, G. Brandl, B. Pedersen, H. Berger, P. Lemmens, and C. Pfleiderer, Phys. Rev. Lett. **108**, 237204 (2012).
[23] S. Seki, J.-H. Kim, D. S. Inosov, R. Georgii, B. Keimer, S. Ishiwata, and Y. Tokura, Phys. Rev. B **85**, 220406 (R) (2012).
[24] S. Seki, S. Ishiwata, and Y. Tokura, Phys. Rev. B **86**, 060403 (2012).
[25] Y. Okamura, F. Kagawa, M. Mochizuki, M. Kubota, S. Seki, S. Ishiwata, M. Kawasaki, Y. Onose, and Y. Tokura, Nat. Commun. **4**, 2391 (2013).
[26] Y. Okamura, F. Kagawa, S. Seki, M. Kubota, M. Kawasaki, and Y. Tokura, Phys. Rev. Lett. **114**, 197202 (2015).
[27] M. Mochizuki, Phys. Rev. Lett. **114**, 197203 (2015).
[28] Y. Onose, Y. Okamura, S. Seki, S. Ishiwata, and Y. Tokura, Phys. Rev. Lett. **109**, 037603 (2012).
[29] T. Schwarze, J. Waizner, M. Garst, A. Bauer, I. Stasinopoulos, H. Berger, C. Pfleiderer, and D. Grundler, Nat. Mater. **14**, 478 (2015).
[30] Model B4350-30C from Southwest Microwave, Inc., www.southwestmicrowave.com.
[31] Y. Wei, S. L. Chin, and P. Svedlindh, J. Phys. D: Appl. Phys. **48**, 335005 (2015).
[32] C. E. Patton, J. Appl. Phys. **39**, 3060 (1968).
[33] D. D. Stancil and A. Prabhakar, *Spin Waves Theory and Applications* (Springer, 2009).
[34] We call it α_{intr} at this point as the parameter is extracted from linear slopes. Later we will argue that standing spin waves exhibit sharp resonances leading to a lower α'_{intr}.
[35] Y. Iguchi, S. Uemura, K. Ueno, and Y. Onose, Phys. Rev. B **92**, 184419 (2015).
[36] V. Vlaminck and M. Bailleul, Phys. Rev. B **81**, 014425 (2010).
[37] M. I. Kobets, K. G. Dergachev, E. N. Khatsko, A. I. Rykova, P. Lemmens, D. Wulferding, and H. Berger, Low Temp. Phys. **36**, 176 (2010).
[38] A. Maisuradze, A. Shengelaya, H. Berger, D. M. Djokić, and H. Keller, Phys. Rev. Lett. **108**, 247211 (2012).
[39] T. J. Silva, C. S. Lee, T. M. Crawford, and C. T. Rogers, J. Appl. Phys. **85**, 7849 (1999).

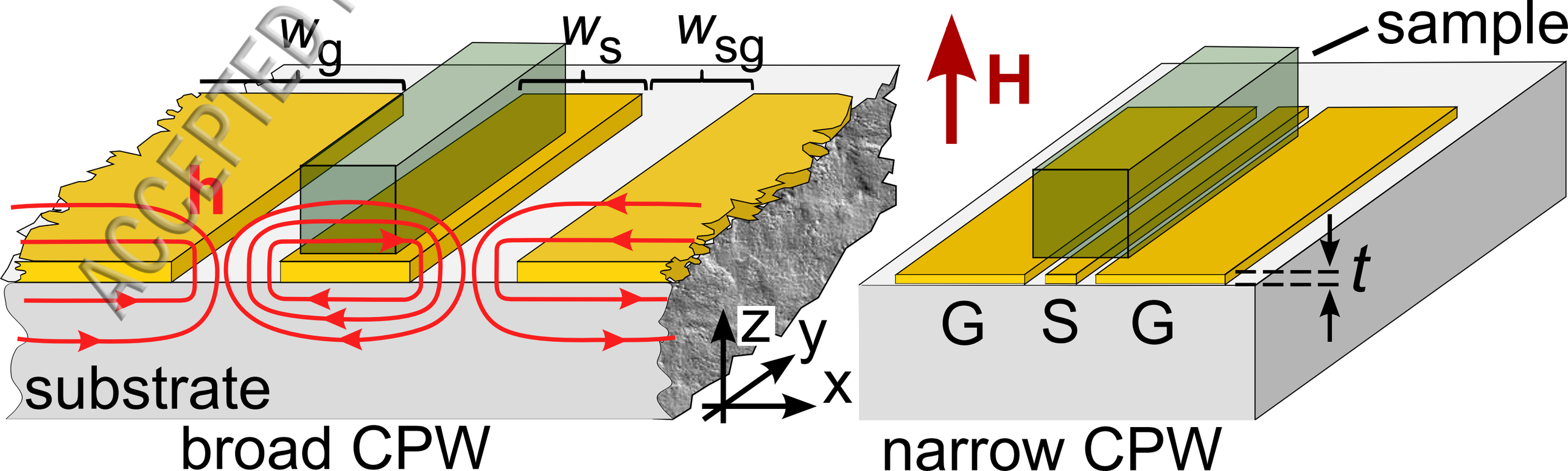
w_g
w_s
w_sg
h
substrate
z
y
x
broad CPW
H
sample
G S G
t
narrow CPW

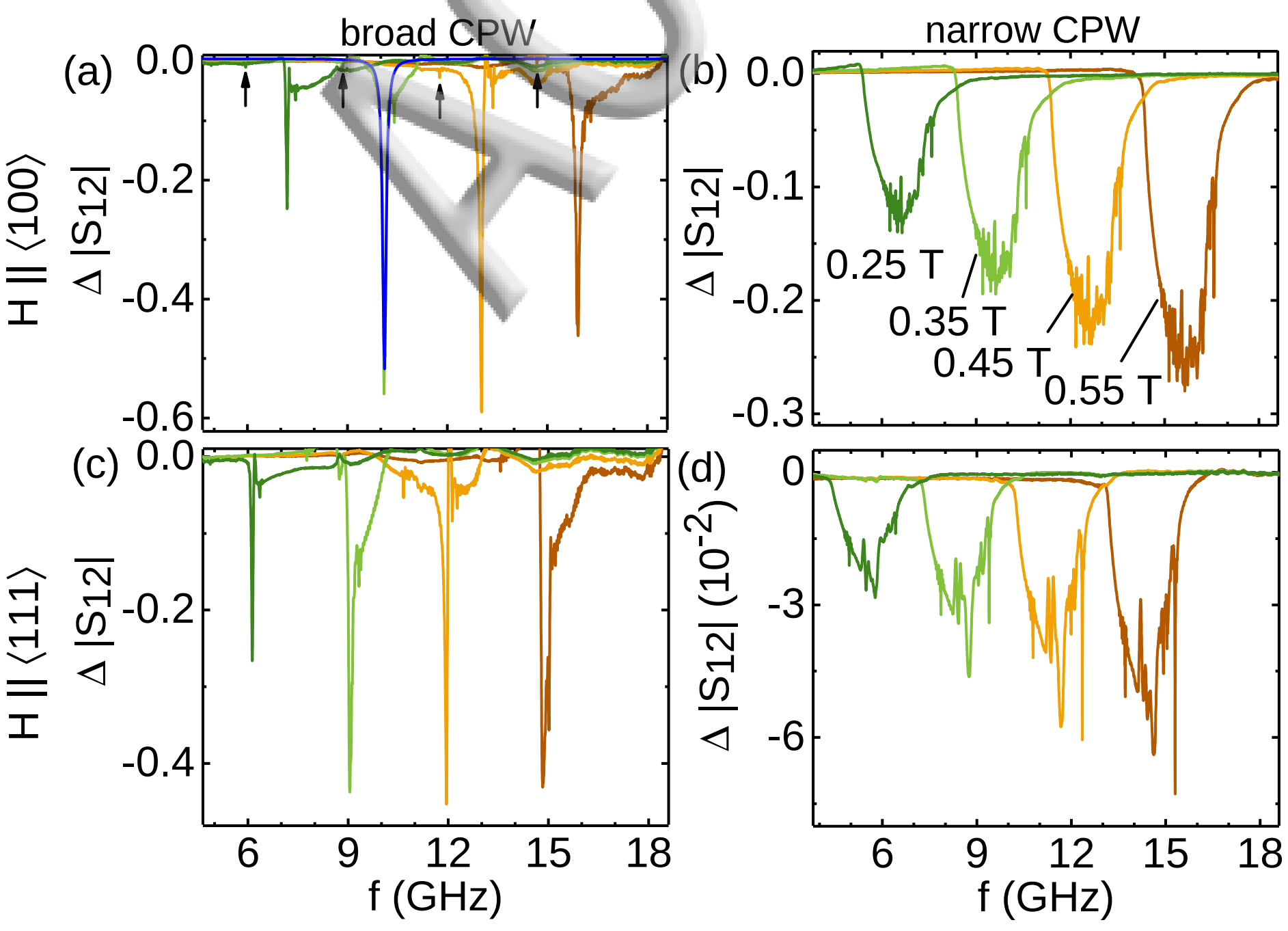
broad CPW
narrow CPW
(a)
(b)
(c)
(d)
H || ⟨100⟩
H || ⟨111⟩
Δ |S12|
Δ |S12| (10-2)
0.0
-0.2
-0.4
-0.6
-0.1
-0.3
0
-3
-6
0.25 T
0.35 T
0.45 T
0.55 T
6
9
12
15
18
f (GHz)

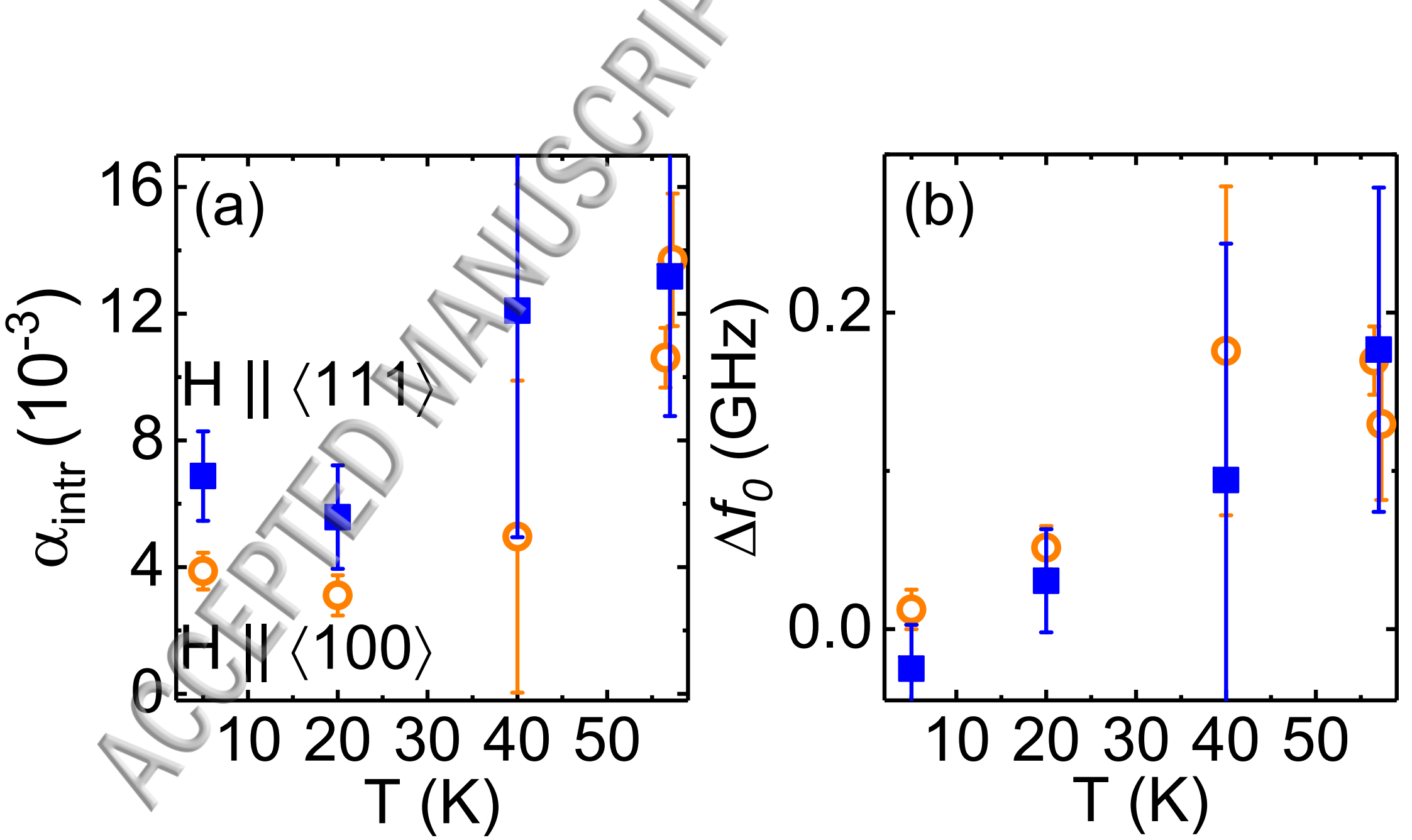

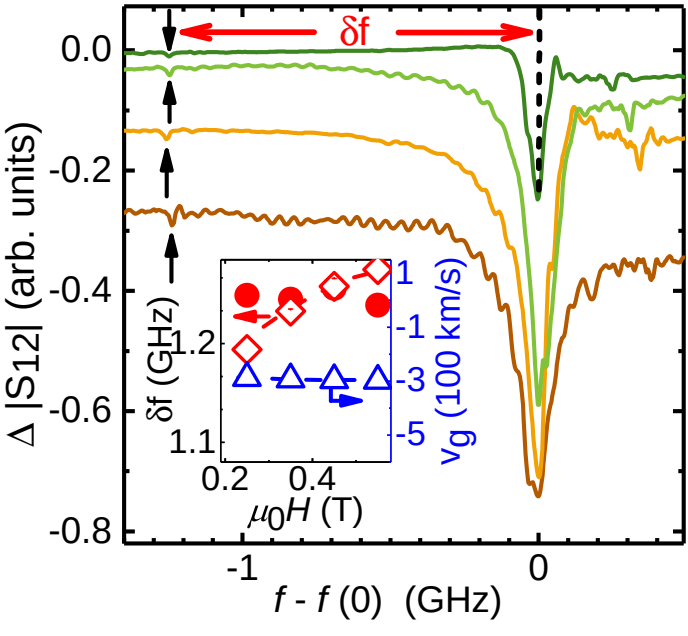
δf
0.0
-0.2
-0.4
-0.6
-0.8
Δ |S12| (arb. units)
-1
0
f - f (0) (GHz)
δf (GHz)
1.2
1.1
0.2
0.4
μ0H (T)
1
-1
-3
-5
vg (100 km/s)

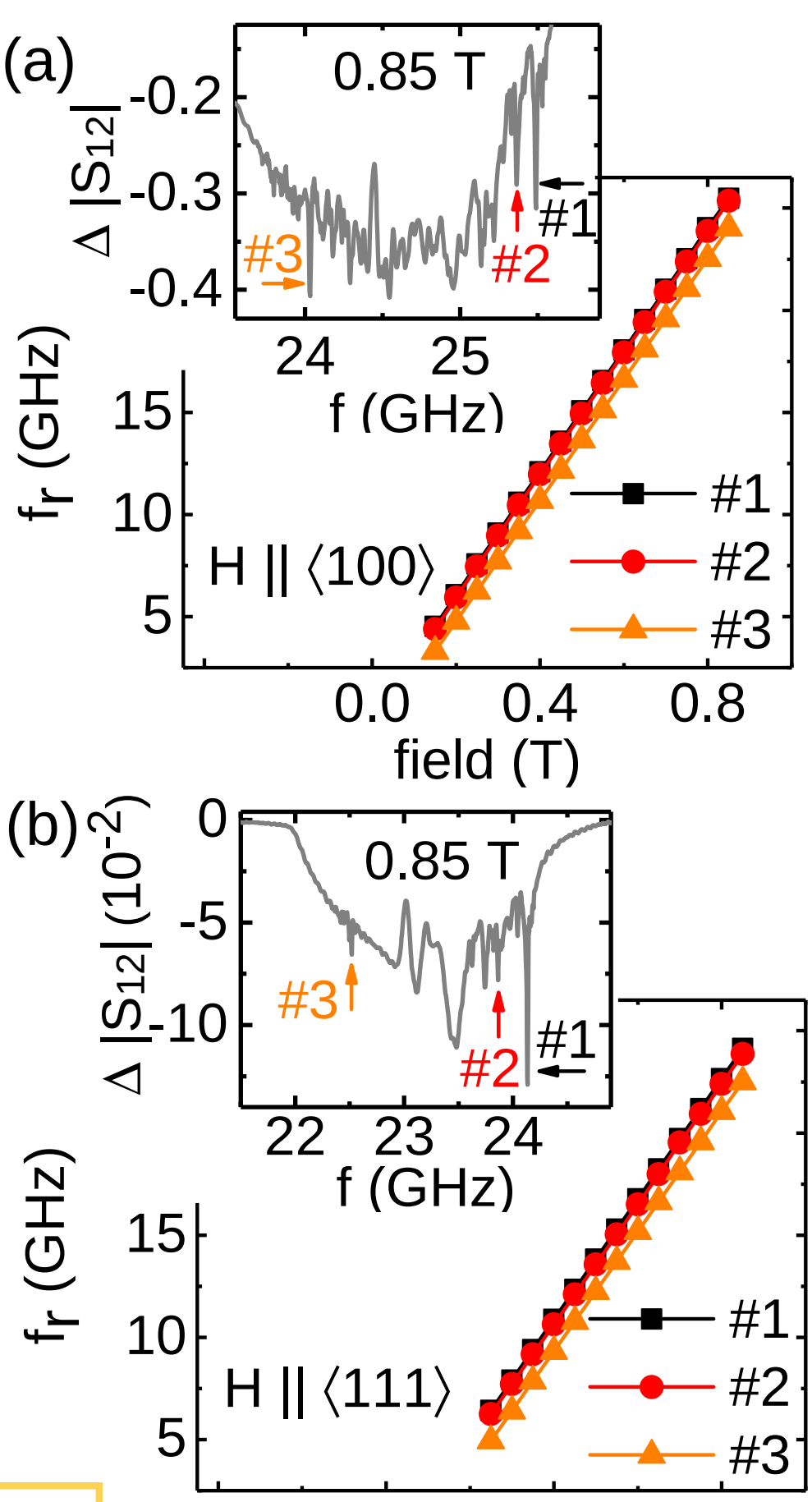

This manuscript was accepted by Appl. Phys. Lett. Click here to see the version of record.